BIOCHEMISTRY
including biophysical chemistry & molecular biology

Article

pubs.acs.org/biochemistry

Femtomolar Inhibitors Bind to 5′-Methylthioadenosine Nucleosidases with Favorable Enthalpy and Entropy

Keisha Thomas,[†] Antti M. Haapalainen,[†] Emmanuel S. Burgos,[†] Gary B. Evans,[‡] Peter C. Tyler,[‡] Shivali Gulab,[‡] Rong Guan,[†] and Vern L. Schramm*[,†]

[†]Department of Biochemistry, Albert Einstein College of Medicine, 1300 Morris Park Avenue, Bronx, New York 10461, United States
[‡]Carbohydrate Chemistry Team, Industrial Research Limited, Gracefield, New Zealand

Supporting Information

ABSTRACT: 5′-Methylthioadenosine/*S*-adenosylhomocysteine nucleosidase (MTAN) catalyzes the hydrolytic cleavage of adenine from methylthioadenosine (MTA). Inhibitor design and synthesis informed by transition state analysis have developed femtomolar inhibitors for MTANs, among the most powerful known noncovalent enzyme inhibitors. Thermodynamic analyses of the inhibitor binding reveals a combination of highly favorable contributions from enthalpic (−24.7 to −4.0 kcal mol^{-1}) and entropic (−10.0 to 6.4 kcal mol^{-1}) interactions. Inhibitor binding to similar MTANs from different bacterial species gave distinct energetic contributions from similar catalytic sites. Thus, binding of four transition state analogues to *Ec*MTAN and *Se*MTAN is driven primarily by enthalpy, while binding to *Vc*MTAN is driven primarily by entropy. Human MTA phosphorylase (*h*MTAP) has a transition state structure closely related to that of the bacterial MTANs, and it binds tightly to some of the same transition state analogues. However, the thermodynamic signature of binding of an inhibitor to *h*MTAP differs completely from that with MTANs. We conclude that factors other than first-sphere catalytic residue contacts contribute to binding of inhibitors because the thermodynamic signature differs between bacterial species of the same enzyme.

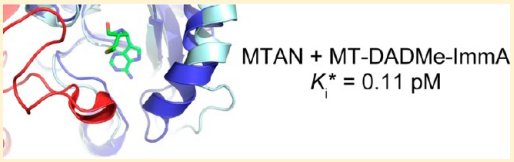

The bacterial enzyme 5′-methylthioadenosine/*S*-adenosylhomocysteine nucleosidase (MTAN) (EC 3.2.2.16) catalyzes the hydrolytic cleavage of 5′-methylthioadenosine (MTA) to form adenine and 5′-methylthioribose (MTR). MTAN inhibition disrupts the production of autoinducers, the chemical messengers required for quorum sensing. The disruption of quorum sensing prevents the coordinated expression of genes responsible for virulence, resulting in attenuated pathogenicity and easier clearance by the immune system.[1−3] MTAN is not present in humans; therefore, it is an attractive target for the design of novel antibacterial drugs. Perturbation of MTAN activity also affects other key cellular pathways, including the activated methyl cycle, polyamine synthesis, and methyltransferase reactions.

The transition states for *Escherichia coli*, *Neisseria meningitidis*, and *Streptococcus pneumoniae* MTANs have been determined by kinetic isotope effect measurements together with quantum chemistry and in silico modeling.[4−6] *E. coli* MTAN (*Ec*MTAN) has a late dissociative (D_N*A_N) transition state with little bond order to the leaving group or the attacking nucleophile, resulting in significant ribocation character.[4] Here we examine the binding of transition state analogues to the *Vibrio cholerae* (*Vc*MTAN), *Salmonella enterica* (*Se*MTAN) and *Escherichia coli* enzymes (EcMTAN). *Vc*MTAN, *Se*MTAN also have kinetic properties consistent with late dissociative transition states as determined by the relative K_i* values for binding of transition state analogues with properties of early or late transition states.[7]

First-generation transition state analogues (Immucillin-A-based) and second-generation transition state analogues (DADMe-Immucillin-A-based) mimic early and late dissociative transition states, respectively (Figure 1).[8] These transition state analogues display slow-onset, tight-binding inhibition with K_i* values in the femtomolar to picomolar range. When compared to the K_m values for the enzymes reported here, the K_m/K_i* ratios are as high as 4.75 × 10^6 (Tables 1 and 2).

Thermodynamic contributions to the binding of high-affinity inhibitors to two nucleoside phosphorylases, human MTA phosphorylase (*h*MTAP) and human purine nucleoside phosphorylase (*h*PNP), have been described previously.[9,10] Transition state theory proposes that chemically stable analogues of the transition state are expected to bind tightly to their cognate enzymes, in a manner proportional to the rate acceleration imposed by the enzyme.[11] The mechanism of this interaction is conversion of the dynamic motions involved in catalysis to thermodynamic interactions, and therefore, transition state analogues convert dynamic catalytic energy into thermodynamic binding energy.[12] Transition state analogues are used here to probe the energetic stabilization of MTAN−transition state analogue complexes, manifested in the form of binding energy. Isothermal calorimetry (ITC) is used to investigate specific thermodynamic contributions to binding as transition state analogues are titrated against various bacterial MTANs.

Received: July 24, 2012
Revised: August 24, 2012
Published: August 29, 2012

   dx.doi.org/10.1021/bi3009938 | *Biochemistry* 2012, 51, 7541−7550

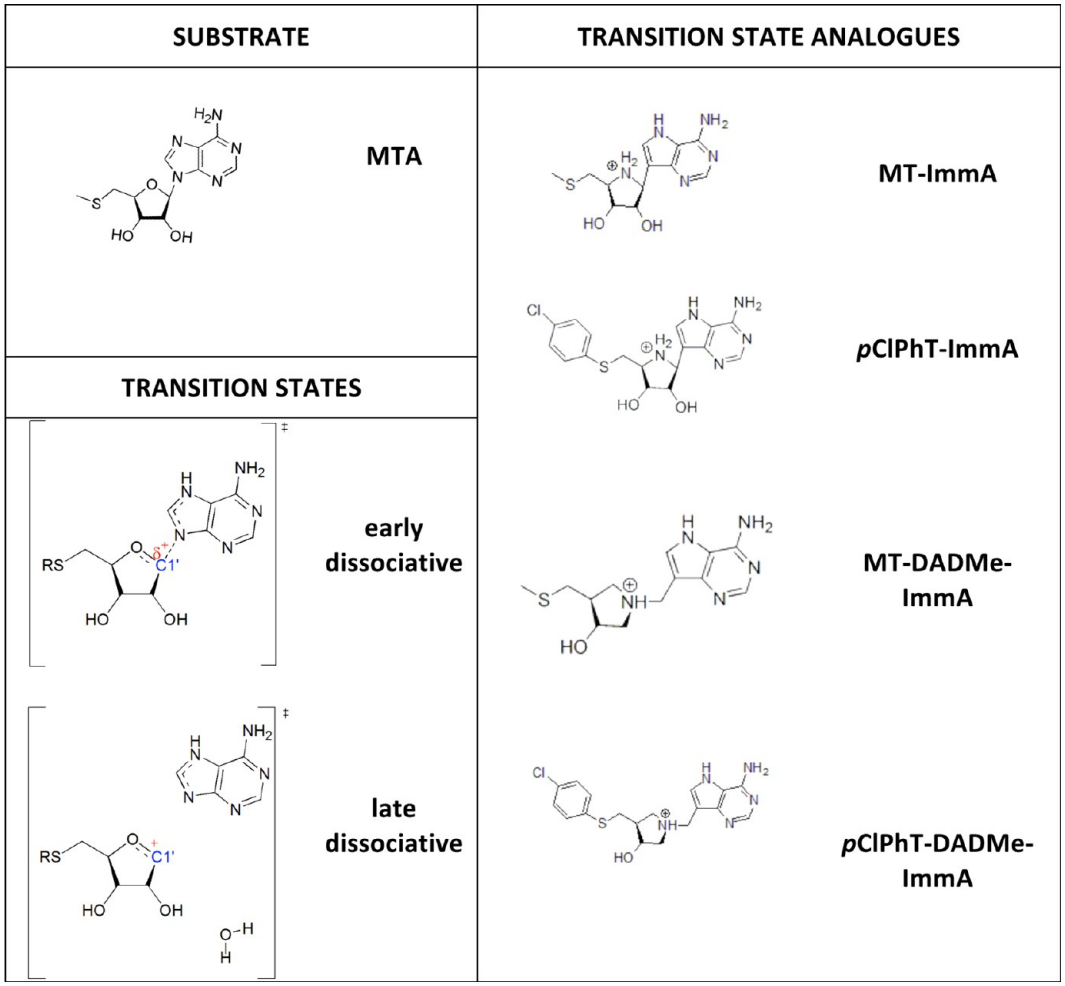

Figure 1. Structure of the substrate MTA, the early and late dissociative transition state analogues, and transition state analogues. The R group in the transition state figures represents a methyl or homocysteine moiety. The early dissociative transition state maintains partial bond order to the leaving group. The late dissociative transition state maintains zero bond order to the leaving group. For more detailed information about the transition states, see refs 4−6.

MATERIALS AND METHODS

Chemicals. Transition state analogue inhibitors were synthesized, purified, and characterized as previously reported.[8,13] [*methylene*-^{14}C]MT-DADMe-ImmA was synthesized with the radiolabel positioned at the methylene bridge carbon. See the Supporting Information for details.

Enzyme Expression. *Ec*MTAN and *Vc*MTAN genomic DNA was isolated using the Maloy DNA extraction method that utilizes a phenol/choloroform/isoamyl alcohol extraction. The region of interest from the isolated DNA was amplified using polymerase chain reaction (PCR). The primers used were flanked by *att*B1 and *att*B2 sites to facilitate use with the Gateway Technology Clonase II System (Invitrogen). The entry clone combines with the *att*R sites in the destination vector (pDEST14) (Invitrogen) to produce the gene of interest flanked by *att*B sites. The recombinant enzymes had a TEV protease cleavable, His_6 N-terminal tag. This adds 12 additional residues to the N-terminal end of the protein for *Ec*MTAN and *Vc*MTAN. The gene encoding *Se*MTAN was synthesized and cloned into the pDONR221 vector (Invitrogen) with DNA 2.0 (Menlo Park, CA), incorporating a His_6 N-terminal tag and terminal *att*B sequences. The gene was then swapped into the pDEST14 vector (Invitrogen) and transformed into BL21(DE3) competent cells (Invitrogen). The following PCR primers were used: *Ec*MTAN forward, GGGGACAAGTTTGTACAAAAAAGCAGGCTACGAAGGAGATAGGATGAAAATCGGCATCATTGGTGC; *Ec*MTAN reverse, GGGGACCACTTTGTACAAGAAAGCTGGGTCTTAGTGATGGTGATGGTGATGACCTTGGAAGTACAGGTTTTCGCCATGTGTGCCAGTTTCTGC; *Vc*MTAN forward, GGGGACAAGTTTGTACAAAAAAGCAGGCTTCGAAGGAGATAGCATGAAAATCGGCATCATCGGCGC; *Vc*MTAN reverse, GGGGACCACTTTGTACAAGAAAGCTGGGTCTTAGTGATGGTGATGGTGATGACCTTGGAAGTACAGATTTTCTTTGAGCAGTTCGACC.

Protein Expression and Purification. *Ec*MTAN, *Se*MTAN, and *Vc*MTAN were transformed into One Shot BL21 Star(DE3) chemically competent cells (Invitrogen). The cells were grown in LB containing 50 μg/mL carbenicillin (37 °C, 220 rpm) to an OD_{600} of 0.6, followed by induction with 0.5 mM IPTG for a further 4 h at 37 °C. Cells were harvested by centrifugation at 4500*g* for 20 min. The cell pellet was suspended in 20 mL of lysis buffer (20 mM TEA and 300 mM NaCl) containing EDTA-free protease inhibitor tablets (Roche Diagnostics, manufacturer protocol followed) and 20 mg of lysozyme. Cells were lysed using a sonicator. The lysed cells were centrifuged at 13000*g* for 30 min. The supernatant was loaded onto a Ni-NTA (Quiagen) column equilibrated in lysis buffer. The protein was eluted from the column using a stepwise

dx.doi.org/10.1021/bi3009938 | *Biochemistry* 2012, 51, 7541−7550

imidazole gradient [in 20 mM TEA and 300 mM NaCl (pH 7.8)] ranging from 25 to 250 mM (increasing in 25 mM increments). The proteins were >95% pure as assessed by sodium dodecyl sulfate−polyacrylamide gel electrophoresis.

Protein Preparation for ITC. Purified MTANs were found to contain adenine bound in their active sites. The tightly bound adenine was removed using dialysis against 100 mM phosphate buffer (pH 7.8) containing 0.5% (v/v) powdered, activated charcoal for 3 days. The enzyme was subsequently dialyzed overnight against 100 mM phosphate buffer (pH 7.8). This dialysate was filtered and saved for use in ITC titrations.

***K*$_m$ Determination.** The K_m values for MTAN with the substrate MTA were determined using the radiolabeled MTA substrate and an HPLC assay for isolation of the labeled adenine. See the Supporting Information for details.

***K*$_i$ Determination.** Inhibitor dissociation constants were measured using a CARY 300 UV−vis spectrophotometer. The adenine formed by the action of MTAN was coupled to xanthine oxidase to form 2,8-dihydroxyadenine. The reactions were conducted at 25 °C, in 1 cm path length cuvettes in a reaction volume of 1 mL. The reaction mixture contained 100 mM HEPES, 50 mM KCl (pH 7.5), 700 μM MTA, 1 unit of xanthine oxidase, and appropriate concentrations of the inhibitor. The reactions were initiated by the addition of 1 nM MTAN. This assay was monitored at 305 nm and has an extinction coefficient of 15.5 mM^{-1} cm^{-1}. Slow-onset inhibition constants in the presence of 10-fold more inhibitor than enzyme were fitted to eq 1:

$$\vartheta_s'/\vartheta_s = \frac{K_m + [S]}{K_m + [S] + K_m[I]/K_i^*} \quad (1)$$

where ϑ_s' and ϑ_s are steady state reaction rates in the presence and absence of inhibitor, respectively, and [S] and [I] are the concentrations of the substrate and inhibitor, respectively. All inhibitors described here exhibited slow-onset inhibition. The slow-onset inhibition constant is reported here as K_i^*, and this value is used to fit the ITC data at the first active site.

Catalytic Site Titration. The concentrations of the MTANs were estimated on the NanoDrop spectrometer using extinction coefficients predicted by the Expasy ProtPram[14] tool as a result of the tagged protein sequence. The extinction coefficients generated using this method include significant error because MTANs do not contain tryptophan; however, it provided working estimates for more quantitative experiments. The concentrations of MTA and MT-DADMe-ImmA were determined using the NanoDrop spectrometer ($\varepsilon_{260,MTA}$ = 15.9 mM^{-1} cm^{-1}, and $\varepsilon_{260,MT\text{-}DADMe\text{-}ImmA}$ = 8.5 mM^{-1} cm^{-1}). Enzyme (20 μM) was incubated with ≤20 μM inhibitor for 1 h at 25 °C, and 10 μL of the enzyme−inhibitor complex was added to a 990 μL solution of 250 μM MTA [100 mM HEPES and 50 mM KCl (pH 7.8)]. The reaction rate was determined as a function of adenine formation at 274 nm ($\varepsilon_{MTA\rightarrow adenine}$ = 1.9 mM^{-1} cm^{-1}) on a CARY 300 UV−vis spectrophotometer at 25 °C. The catalytic site titration data for *Ec*MTAN and *Vc*MTAN was fitted using a linear regression function, while the titration data for *Se*MTAN were fitted using a segmental linear regression function (Prism5, GraphPad).

Determination of *k*$_{off}$. [*methylene bridge*-^{14}C]MT-DADMe-ImmA (I*, 50 μM) was incubated with 50 μM enzyme for 2 h at 25 °C in a 200 μL volume to form enzyme−inhibitor* (E−I*) complexes in 100 mM HEPES and 50 mM KCl (pH 7.5). After 2 h, 10 μL of the E−I* complex was removed and mixed with 50 μL of HEPES. The solution was centrifuged in Amicon Ultra Centrifugal Filter units (Millipore) with a 10K molecular weight cutoff (13200 rpm for 5 min). The enzyme and enzyme-bound ligands were retained, while the supernatant contained free inhibitor. The ultrafiltrate (15 μL) was added to scintillation vials, dried on a speed-vac, mixed with 10 mL of scintillation fluid (PerkinElmer), and counted in Tricarb 2910 TR instrument (PerkinElmer) for 5 min. Excess unlabeled MT-DADMe-ImmA (17 mM) was added to the E−I* complex reaction mixture to a final concentration of 5 mM. Aliquots of the reaction mixture (10 μL) were removed at the desired times, and the radioactivity in the ultrafiltrate was measured as described above. Counts were corrected for the count dilution after addition of excess MT-DADMe-ImmA ($[I]_{counts,corrected}$). The amount of bound inhibitor ($[I]_{bound}$ or B) was calculated as follows:

$$[I]_{bound} = [I]_{max} - [I]_{counts,corrected}$$

where $[I]_{max}$ represents the maximal calculated counts in 10 μL if all I* were free in solution. Data were fitted to the equation for a first-order reaction, $\ln(B/B_0) = -kt$, where B_0 represents the amount of bound inhibitor before dilution.

Isothermal Titration Calorimetry Studies. ITC studies were conducted using a VP-ITC (MicroCal) microcalorimeter. Inhibitors were dissolved in the dialysate from the protein preparation, and all solutions were filtered (Millipore, 0.2 μm). All solutions were degassed (Microcal Thermovac) for 15 min. The reference cell was filled with dialysate; 1.5 mL of enzyme was loaded into the sample cell, and 250 μL of the inhibitor solution was loaded into the injection syringe. Titration injection volumes ranged from 4 to 7 μL. All titrations were conducted at 25 °C.

Data Processing of ITC. ITC data were fitted using the equations provided in Origin7 that describe two distinct independent binding sites. Tight-binding inhibitors cannot be analyzed by these equations, and for tight-binding data, accurate K_i^* values obtained from kinetic analysis were used to fit the ITC data. The K_i^* values were used in eq 2 to generate ΔG. ΔH is the integral of the power needed to maintain the temperature of the sample cell at the same temperature as the reference cell after injection. The entropy term was determined using the Gibbs free energy equation (eq 3).

$$\Delta G = RT \ln K_i^* \quad (2)$$

$$\Delta G = \Delta H - T\Delta S \quad (3)$$

For more weakly bound ligands, the heat content (Q) after any injection is calculated using eq 4

$$Q = M_t V_0(\eta_1\Theta_1\Delta H_1 + \eta_2\Theta_2\Delta H_2) \quad (4)$$

where M_t is the concentration of the enzyme, V_0 is the volume of the sample cell, n represents the number of active sites, and Θ represents the fraction of active sites occupied by ligand. The heat effect for the ith injection is represented by eq 5, which corrects for the change in volume after each injection.

$$\Delta Q(i) = Q(i) + \frac{dV_t}{V_0}\left[\frac{Q(i) + Q(i-1)}{2}\right] - Q(i-1) \quad (5)$$

Data fitting involved initial estimates of n and K_a (association constant of inhibition, taken as the reciprocal of equilibrium dissociation constant K_i^*). The standard errors in enthalpy were derived directly from the fit of the data generated due to heats of binding. The standard errors for the free energy terms were calculated on the basis of the error in the K_i^* values used to fit the data. The standard errors of the entropy terms were calculated using standard error propagation methodology assuming zero

dx.doi.org/10.1021/bi3009938 | *Biochemistry* 2012, 51, 7541−7550

correlation between errors. More detailed information about data fitting can be attained from the MicroCal user manual.

Determination of Cavity Volumes. The cavities and pockets were identified with the PyMOL Molecular Graphics System using seven solvent radii and three solvent radii as a cavity detection radius and cavity detection cutoff, respectively.

Hydrogen Bonding Network between Ribose and Water in *Ec*MTAN. The lengths of the hydrogen bonds were determined using Coot.[15]

ITC Isotherm Comparison. The data for the titration of *h*MTAP and *h*PNP (Figure 10a) used published data[9,10] for comparison with the raw data from the titration of *Ec*MTAN with MT-DADMe-ImmA.

RESULTS

Kinetic Constants for Transition State Analogues. MTAN enzymes bind tightly to their substrates and are highly active catalysts with catalytic efficiency values (k_{cat}/K_m) of > 10^7 M^{-1} s^{-1} (Table 1). The Immucillin-A and DADMe-Immucillin-A inhibitors exhibit tight binding to the MTANs with slow onset K_i* values as low as 40 fM (Table 2). These inhibitors capture key characteristics of the transition states of bacterial MTANs and represent some of the tightest binding inhibitors known in enzymology.

Table 1. Kinetic Constants for Related MTANs

organism	K_m (nM)	k_{cat} (s^{-1})	k_{cat}/K_m ($\times 10^7$ M^{-1} s^{-1})
E. coli	190 ± 20	2.3 ± 0.1	1.2
S. enterica	400 ± 20	20 ± 0.5	5.0
V. cholerae	360 ± 10	4.2 ± 0.3	1.2

Table 2. Equilibrium Dissociation Constants for Transition State Analogues of MTANs

analogue	*E. coli* K_i* (pM)	*S. enterica* K_i* (pM)	*V. cholerae* K_i (pM)
MT-ImmA	89 ± 13	274 ± 18	300 ± 24
*p*ClPhT-ImmA	5.5 ± 0.6	38.0 ± 2.2	59 ± 9.8
MT-DADMe-ImmA	0.11 ± 0.01	5.0 ± 0.4	12.5 ± 3.7
*p*ClPhT-DADMe-ImmA	0.04 ± 0.01	2.7 ± 0.7	9.3 ± 2.0

Catalytic Equivalence at MTAN Active Sites. MTAN was titrated with substoichiometric amounts of tight-binding inhibitor MT-DADMe-ImmA followed by the determination of the catalytic activity of the free active sites. The inhibitor:MTAN ratio indicates the number of inhibitor molecules bound per dimer. At inhibitor:MTAN dimer ratios of 2.43 ± 0.12, 2.23 ± 0.07, and 1.04 ± 0.03 for *E. coli*, *V. cholerae*, and *S. enterica* MTANs, respectively, catalytic activity is completely or partially abolished (Figure 2). The active sites of *Ec*MTAN and *Vc*MTAN are catalytically independent. *Se*MTAN has cooperative active sites. As the first active site is occupied, activity at the second active site was reduced by >4-fold.

Dissociation of MT-DADMe-ImmA from MTANs. The DADMe-ImmA inhibitors mimic the late dissociative transition state of *Ec*MTAN, *Se*MTAN, and *Vc*MTAN. MT-DADMe-ImmA binds to these MTANs with K_i* values ranging from 0.11 to 12.5 pM (Table 2). Their tight binding is related to slow rates of release from the protein, and we measured the rates by diffusional exchange. Following preincubation of the enzyme with a radiolabeled inhibitor (I*), excess unlabeled inhibitor (I) was added and the rate of I* dissociation was measured. The dissociation rates for *Ec*MTAN, *Se*MTAN, and *Vc*MTAN gave k_{off} values of 3.47×10^{-3}, 1.15×10^{-3}, and 4.73×10^{-3} min^{-1}, respectively (Figure 3). The inhibitor dissociates from the enzyme with half-times ($t_{1/2}$) of 3.3, 7.4, and 2.4 h for *Ec*MTAN, *Se*MTAN, and *Vc*MTAN, respectively.

Isothermal Calorimetry Studies. ITC data for titrations performed with early (MT-ImmA and *p*ClPhT-ImmA) and late (MT-DADMe-ImmA and *p*ClPhT-DADMe-ImmA) transition state analogues were fitted using slow-onset K_i* values to establish the binding constant for the first active site (Table 3). All titrations were performed until both active sites were occupied, and further titration led only to serial heats of dilution (Figure 4).

ITC Profiles for Binding of First-Generation Immucillin-A Inhibitors. All isotherms indicate both favorable enthalpy and entropy at the first binding site with the exceptions of the enzyme/ligand titrant pairs: *Se*MTAN/MT-ImmA and *Ec*MTAN/*p*ClPhT-DADMe-ImmA. An entropic penalty of 2.3 kcal mol^{-1} for the *Se*MTAN/MT-ImmA titration is consistent with a relatively large K_i* value compared to those of most other titrant pairs in this study (Table 2). For the *Ec*MTAN/*p*ClPhT-DADMe-ImmA pair, the entropic penalty of 6.4 kcal/mol is relatively modest when compared to the extremely large enthalpic contribution of −24.7 kcal/mol.

Titrations of first-generation inhibitors against *Ec*MTAN and *Se*MTAN displayed enthalpy-driven binding with negative cooperativity as the second active sites are filled. Titration of MT-ImmA to *Vc*MTAN displayed apparent negative single-site enthalpic cooperativity, with small energetic changes as the first active site is filled, followed by no cooperativity as the second active site is filled (Figure 4). Titration of *p*ClPhT-ImmA to *Vc*MTAN also displayed negative cooperativity at the first active

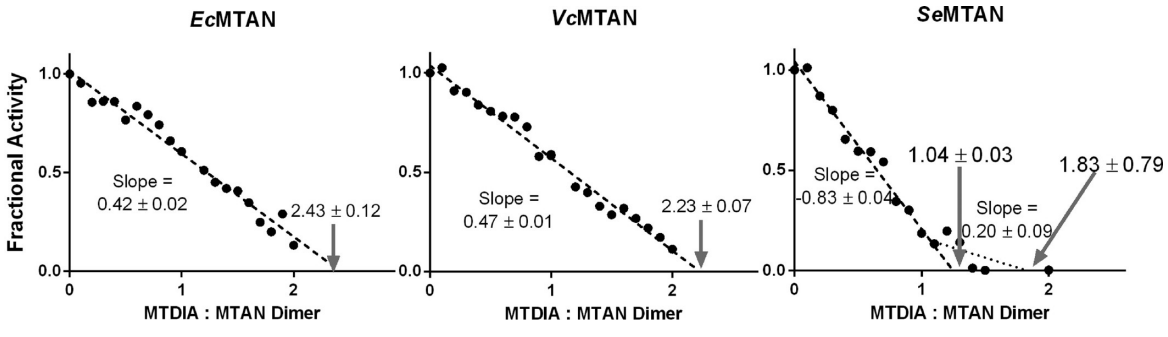

Figure 2. Fractional activity of MTANs with stoichiometric titrations of MT-DADMe-ImmA.

dx.doi.org/10.1021/bi3009938 | *Biochemistry* 2012, 51, 7541−7550

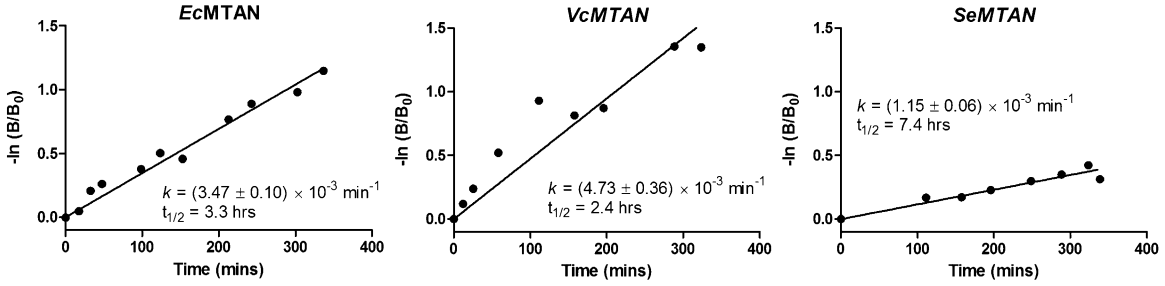

Figure 3. Rates of dissociation (k_{off}) of MT-DADMe-ImmA from MTANs.

Table 3. Thermodynamic Constants for Binding of Transition State Analogues to MTANs

analogue	n^a	ΔG^b (kcal mol^{-1})	ΔH^c (kcal mol^{-1})	$-T\Delta S^d$ (kcal mol^{-1})
		E. coli MTAN		
MT-ImmA	0.94 ± 0.14	−13.7 ± 0.09	−13.0 ± 1.5	−0.7 ± 1.5
	1.02 ± 0.14	−12.5	−8.5 ± 1.3	−4.0
*p*ClPhT-ImmA	0.92 ± 0.06	−15.3 ± 0.06	−9.5 ± 0.08	−5.9 ± 0.1
	1.04 ± 0.06	−11.6	−8.8 ± 0.08	−2.8
MT-DADMe-ImmA	0.99 ± 0.03	−17.7 ± 0.07	−15.2 ± 0.1	−2.5 ± 0.1
	1.04 ± 0.03	−10.1	−13.5 ± 0.2	3.4
*p*ClPhT-DADMe-ImmA	1.08 ± 0.04	−18.3 ± 0.1	−24.7 ± 0.2	6.4 ± 0.2
	0.94 ± 0.04	−10.9	−22.9 ± 0.2	12
		S. enterica MTAN		
MT-ImmA	0.96 ± 0.04	−13.0 ± 0.04	−15.3 ± 0.2	2.3 ± 0.2
	0.94 ± 0.04	−11.2	−11.7 ± 0.3	0.5
*p*ClPhT-ImmA	1.40 ± 0.08	−14.2 ± 0.03	−13.4 ± 1.0	−0.8 ± 1.0
	0.68 ± 0.08	−13.6	−8.8 ± 2.4	−4.8
MT-DADMe-ImmA	1.12 ± 0.06	−15.4 ± 0.05	−12.5 ± 0.06	−2.9 ± 0.08
	0.92 ± 0.04	−11.4	−11.9 ± 0.08	0.5
*p*ClPhT-DADMe-ImmA	0.78 ± 0.04	−15.8 ± 0.2	−11.2 ± 0.1	−4.6 ± 0.2
	1.18 ± 0.06	−11.6	−11.5 ± 0.1	−0.1
		V. cholerae MTAN		
MT-ImmA	0.94 ± 0.02	−13.0 ± 0.05	−4.9 ± 0.08	−8.1 ± 0.1
	0.98 ± 0.02	−10.5	−1.5 ± 0.09	−9.0
*p*ClPhT-ImmA	0.80 ± 0.04	−14.0 ± 0.1	−4.0 ± 0.1	−10.0 ± 0.1
	1.34 ± 0.04	−10.6	−2.1 ± 0.1	−8.5
MT-DADMe-ImmA	1.16 ± 0.04	−14.9 ± 0.2	−6.0 ± 0.2	−8.9 ± 0.3
	0.84 ± 0.04	−13.4	−2.7 ± 0.3	−10.7
*p*ClPhT-DADMe-ImmA	1.36 ± 0.28	−15.0 ± 0.1	−5.3 ± 0.3	−9.7 ± 0.3
	0.68 ± 0.16	−14.1	−3.9 ± 0.9	−10.2

[a] *n* represents the fraction of total sites per dimer giving the indicated enthalpic and associated thermodynamic properties using the best fit described in Materials and Methods (each monomer of the dimer has a single active site). [b] ΔG was calculated from the K_i^* (Table 2) using the equation $\Delta G = RT \ln K_i^*$. [c] ΔH was determined from the ITC titrations of the enzyme with the inhibitor for each of the two catalytic site of the enzyme dimer. [d] $-T\Delta S$ was calculated from the Gibbs free energy equation. All titrations were performed at 25 °C.

site, followed by positive cooperativity as the second active site is filled. Single-site negative cooperativity with small enthalpy effects suggests inhibitor-dependent protein aggregation effects at these protein concentrations specifically for *Vc*MTAN, as normal binding models do not account for these data. As enthalpic changes are small for *Vc*MTAN titrations, the entropy term provides the major contribution to the free energy of binding to the first-generation inhibitors.

ITC Profiles for Binding of Second-Generation DADMe-Immucillin-A Inhibitors. The binding isotherms for titration of the DADMe-ImmA-based inhibitors to the MTANs all exhibit negative cooperativity in enthalpic contributions as the second active sites are filled (Figures 4−6). The ΔG values for binding for DADMe-ImmA-based inhibitors to *Ec*MTAN, *Se*MTAN, and *Vc*MTAN range from −18.3 to −14.9 kcal mol^{-1} as the first active site of the homodimer is filled. Consistent with the trend for binding to first-generation inhibitors; *Ec*MTAN and *Se*MTAN display enthalpy-driven binding while *Vc*MTAN displays entropy-driven binding.

Thermodynamic Binding Profile. Binding of inhibitors to *Ec*MTAN and *Se*MTAN was driven by a large and favorable enthalpy. The average ΔH (ΔH_{avg}) was −14.4 kcal mol^{-1} and the average $-T\Delta S$ ($-T\Delta S_{avg}$) −1.1 kcal mol^{-1} for binding to *Ec*MTAN and *Se*MTAN. Binding of TS analogues to *Vc*MTAN was driven by a favorable entropy. The average ΔH_{avg} was −5.0 kcal mol^{-1} and the average $-T\Delta S_{avg}$ −9.2 kcal mol^{-1} for binding to *Vc*MTAN (Figure 5).

Enthalpy−Entropy Compensation. The enzyme−inhibitor systems in this study display enthalpy−entropy compensation. Systems with a large favorable enthalpy have a smaller favorable entropy (or an entropic penalty in the cases of *Ec*MTAN/*p*ClPhT-DADMe-ImmA and *Se*MTAN/MT-ImmA pairs).

dx.doi.org/10.1021/bi3009938 | *Biochemistry* 2012, 51, 7541−7550

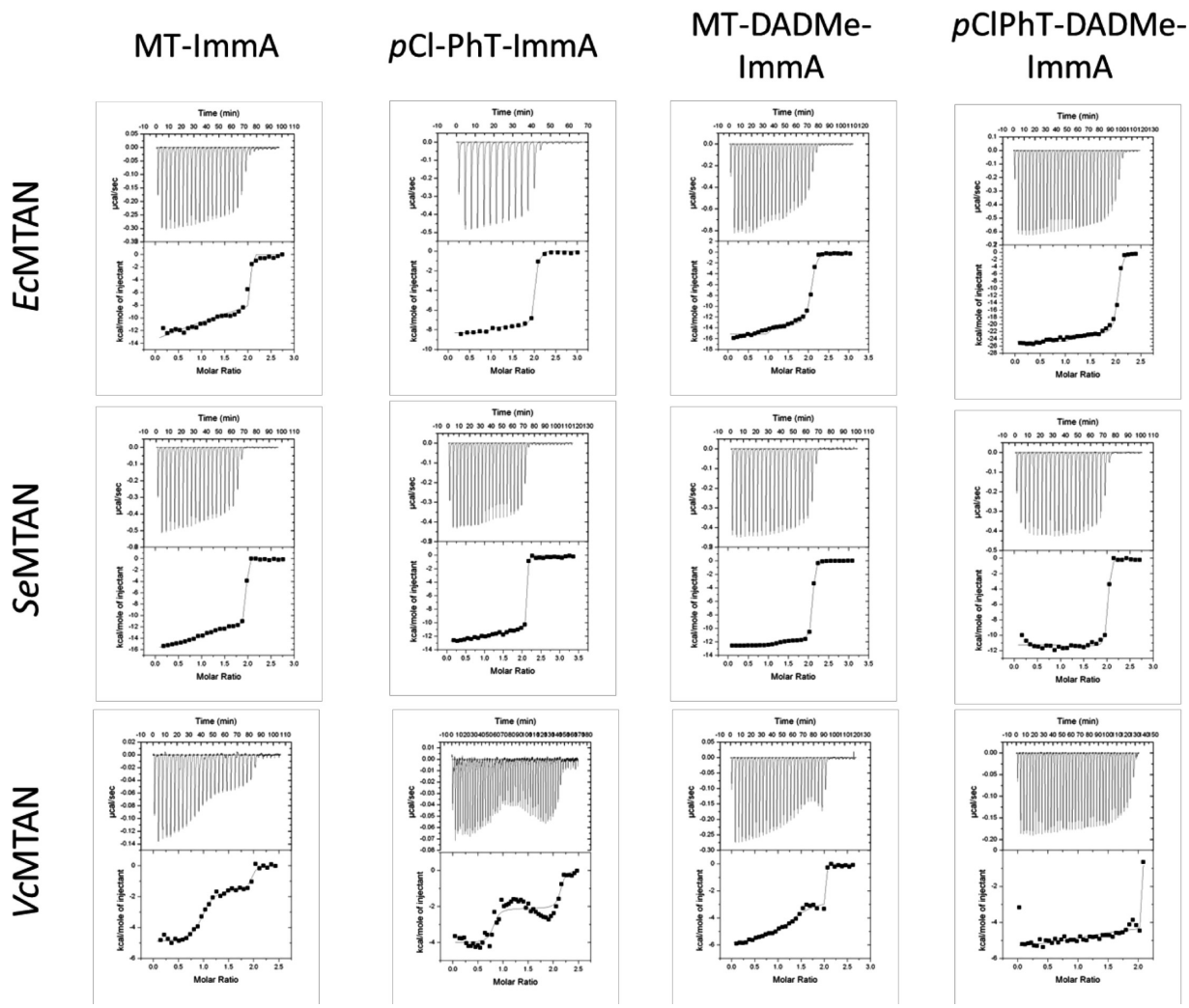

Figure 4. Saturation titration curves for binding of *Ec*MTAN, *Se*MTAN, and *Vc*MTAN to first- and second-generation transition state analogues. All titrations were performed at 25 °C. Titrations were fit to the equation for two independent binding sites, and the solid line is the best fit of the data to that equation. The molar ratio represents the ligand concentration:enzyme dimer concentration ratio. The shape of the binding isotherm for each enzyme–inhibitor system reveals details about binding cooperativity. If the energy released by a subsequent injection is smaller than that of the previous injection, the isotherm indicates a system with negative cooperativity. The opposite is true for a system that displays positive cooperativity. See Table 3 for detailed information about the thermodynamic constants associated with the data.

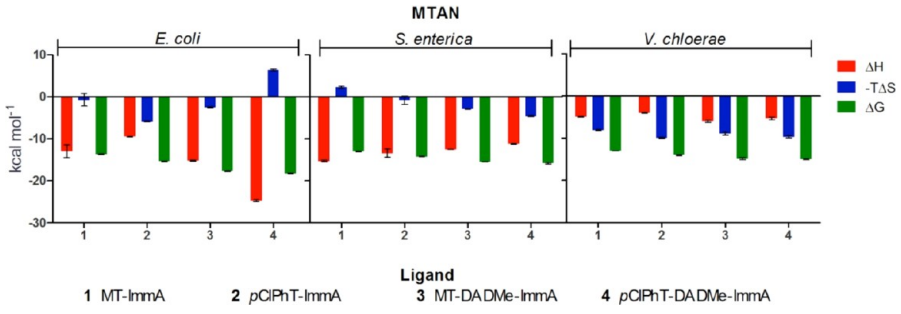

Figure 5. Thermodynamic profiles of ΔH, $-T\Delta S$, and ΔG for the binding of first- and second-generation inhibitors to the first active sites of *Ec*MTAN, *Se*MTAN, and *Vc*MTAN.

Systems with large and favorable entropy terms have a reduced favorable enthalpy. A plot of $-T\Delta S$ versus ΔH generates a best-fit line that indicates this enthalpy–entropy compensation (Figure 6). Titrations of *Se*MTAN and *Vc*MTAN with MT-ImmA represent instances where the enthalpy and/or entropy deviates from the best-fit line in an unfavorable manner. Titration of *Ec*MTAN with MT-DADMe-ImmA indicates deviation from the enthalpy–entropy compensation best-fit line in a favorable manner in terms of enthalpy and/or entropy. These deviations from the best-fit line establish the thermodynamic profile for strong and weaker binding affinity for specific enzyme–inhibitor complexes.

dx.doi.org/10.1021/bi3009938 | *Biochemistry* 2012, 51, 7541–7550

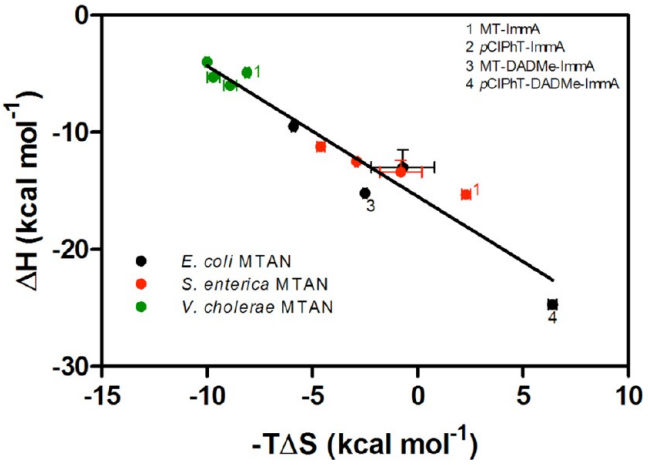

Figure 6. Enthalpy−entropy compensation graph displaying the enthalpy term (ΔH) vs the entropy term ($-T\Delta S$) for each of the MTAN−inhibitor interactions at the first binding site. The standard errors for the enthalpy and entropy terms are represented in this figure for all points. The solid line represents the best-fit line for the data. Note the extraordinary range in the enthalpy term (ΔH) from −4 to −25 kcal/mol.

DISCUSSION

The stoichiometric, tight-binding of transition state analogues to MTANs make these compounds of interest to reveal the energetics of binding.

Although tight-binding occurs at both of the dimer active sites, negative cooperativity is seen in every enzyme-inhibitor case for second site binding, ranging from 0.2 to 7.6 kcal mol^{-1} loss of ΔG binding energy (Table 3). Negative cooperative binding is usually characterized by favorable entropy with a penalty in enthalpy suggesting distortion of the enzyme from its preferred geometry upon binding to the first ligand.[16] Despite the negative cooperativity, the second active site retains sufficient binding energy to result in slow-release kinetics (Figure 3).

Inhibition of the first catalytic site in *Ec*MTAN and *Vc*MTAN leaves the second site with equivalent catalytic activity under saturating substrate conditions (Figure 2). Crystal structures of *Ec*MTAN and *Vc*MTAN complexed with BuT-DADMe-ImmA indicate structural similarity with a root-mean-square deviation of only 0.4 Å between the Cα main chain atoms.[17] *Se*MTAN differs in that saturation of the first active site causes the second site to exhibit less catalytic activity (Figure 2).

The slow rate of inhibitor dissociation from MTANs, reflects the tight binding and the multiple contacts between the enzyme and inhibitor.[18] Determination of off rates has been proposed to be a better predictor of selectivity and efficacy in vivo than determination of equilibrium dissociation constants.[19] On the basis of the measured k_{off}, and the dissociation constants, the calculated k_{on} values for *Vc*MTAN and *Se*MTAN are approximately 10^6 M^{-1} s^{-1}, while the k_{on} for *Ec*MTAN approaches the limit of diffusion at 10^8 M^{-1} s^{-1}. These values represent release rates from the weaker second site under our experimental exchange conditions (Figure 3).

The favorable enthalpy upon transition state analogue binding reflects the ability of these inhibitors to capture key elements of the transition state to form favorable hydrogen bonds and van der Waals interactions. When *Ec*MTAN binds to transition state analogues, the

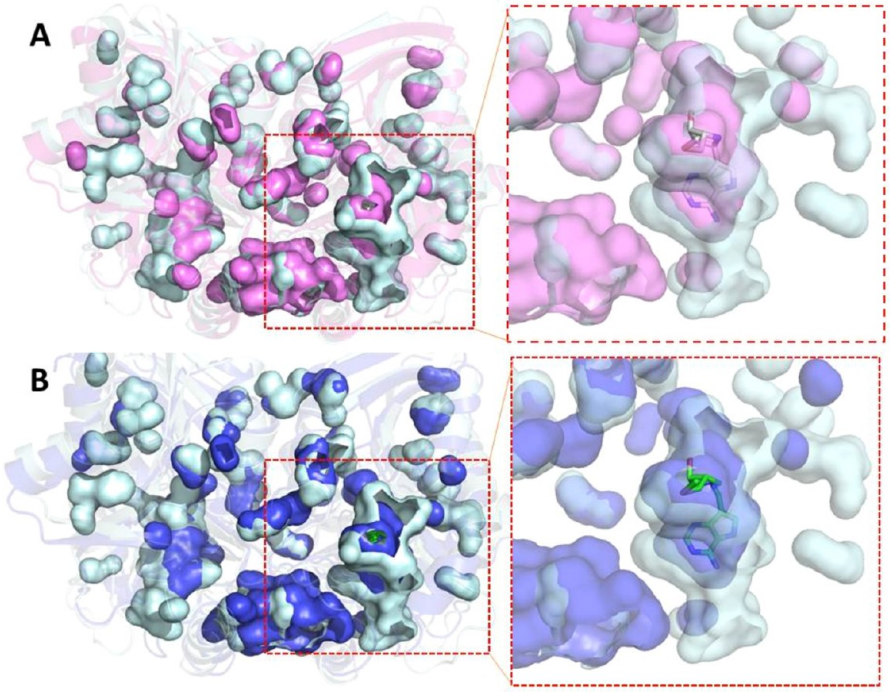

Figure 7. Cavities found in apo and inhibitor-bound *Ec*MTAN. Apo *Ec*MTAN (cyan, PDB entry 1Z5P), *Ec*MTAN complexed with MT-ImmA (pink, PDB entry 1Y6R), and *Ec*MTAN complexed with MT-DADMe-ImmA (blue, PDB entry 1Y6Q) are shown. (A) Cavities of apo *Ec*MTAN (cyan) overlaid with those of the *Ec*MTAN/MT-ImmA pair (pink). The surrounding secondary structure for each enzyme is represented as a ribbon. The close-up shows an overlay of the active site cavities. The apo *Ec*MTAN cavity has a larger volume than the *Ec*MTAN active site cavity that is liganded with MT-ImmA. (B) Cavities of apo *Ec*MTAN (cyan) overlaid with those of the *Ec*MTAN/MT-DADMe-ImmA pair (blue). The surrounding secondary structure for each enzyme is represented as a ribbon. The close-up shows an overlay of the active site cavities. The apo *Ec*MTAN cavity has a larger volume that the *Ec*MTAN active site cavity that is liganded with MT-DADMe-ImmA.

dx.doi.org/10.1021/bi3009938 | *Biochemistry* 2012, 51, 7541−7550

protein condenses (Figure 7). This tightening of the enzyme facilitates stronger electrostatic contacts within the enzyme and at the catalytic sites between the enzyme and inhibitor. Thus, the size of the active site cavity in apo *Ec*MTAN is larger than that in *Ec*MTAN complexed with MT-ImmA or MT-DADMe-ImmA (Figure 7).

The expected loss of favorable entropy due to a more compact liganded system is offset by gains in solvent and protein reorganization (all inhibitors display slow-onset kinetics). When an inhibitor binds, rotational and translational degrees of freedom are also lost in the inhibitor, an unfavorable entropic contribution. Despite these known unfavorable entropic contributions, the favorable system entropy indicates that there is sufficient water reorganization influenced by events at the active site for a favorable entropic contribution to binding.

The enthalpic contributions to inhibitor binding are more obvious because the complex is stabilized in the active site by a hydrogen bonding network formed between protein and water molecules. *Ec*MTAN complexed with MT-DADMe-ImmA has two more structurally resolved water molecules involved in the hydrogen bonding network and several more hydrogen bonds to the inhibitor than MT-ImmA does, readily accounting for the 2200-fold tighter binding of MT-DADMe-ImmA (Figure 8).

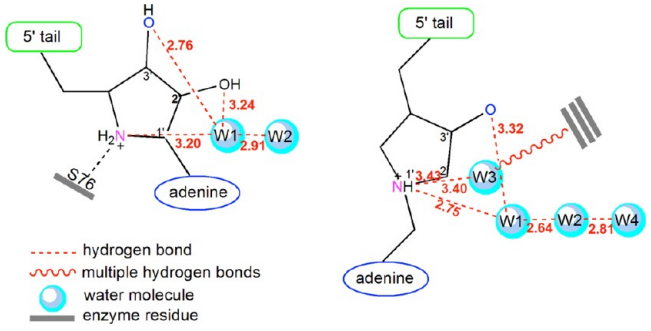

Figure 8. Hydrogen bonding network schematic for the transition state ribocation mimic and structural water molecules in *Ec*MTAN. The pink nitrogens occupy the same positions in the active sites of both complexes. The blue oxygen atoms also occupy the same positions in the active sites. At the left are shown hydrogen bonds to water molecules in the active site of the *Ec*MTAN/MT-ImmA pair (PDB entry 1Y6R). A total of four hydrogen bonds involving water molecules are formed with an additional hydrogen bond to Ser76. At the right are shown hydrogen bonds made to water molecules in the active site of the *Ec*MTAN/MT-DADMe-ImmA pair (PDB entry 1Y6Q). A total of six hydrogen bonds are made to water molecules in the active site. Additional hydrogen bonds made between the waters and enzymatic residues are detailed in the PDB.

Crystal structure analysis indicates that in the active site of *Ec*MTAN (PDB entry 1Y6Q) the methylthio of MT-DADMe-ImmA is surrounded by hydrophobic residues, including Ile50(A), Phe207(A), Val102(B), and Phe105(B). Val102 and Phe105 are residues of the neighboring monomer B of the dimer that contribute to the formation of the substrate binding site of monomer A. The side chain of Phe105(B) forms a hydrophobic interaction with the methylthio group of MT-DADMe-ImmA. The hydrophobic interactions in the regions surrounding the methylthiol or *p*-chlorphenylthio groups of inhibitors may contribute differently to the thermodynamics of binding because this hydrophobic region in *Ec*MTAN is not completely conserved in *Vc*MTAN or *Se*MTAN. For example, Pro113 is part of the hydrophobic region in *Ec*MTAN and *Se*MTAN but is replaced with Ala113 in *Vc*MTAN (Figure S1 of the Supporting Information). How these regions differ in structural detail awaits more complete crystallographic analysis of *Se*MTAN.

When a substrate or inhibitor binds, there are major catalytic site rearrangements in *Ec*MTAN. One dramatic movement involves the loop adjacent to the C-terminal helix, which moves toward the ligand and closer to the active site (Figure 9). Once the loop is placed into this closed conformation, part of it reorganizes to adopt a helical structure, thereby extending the length of the C-terminal helix. This conformational change may be part of the conformational ensemble that gives rise to slow-onset kinetics.[20,21] The closed conformations of enzymes can be expected to expel water, causing the active site to become more hydrophobic, strengthening hydrophobic contacts, and contributing to a more favorable system entropy.

The loop to helix movement, in addition to closing the active site, also extends the dimeric interface interactions. For example, in the ligand-bound conformation of *Ec*MTAN, His204 at the N-terminus of the C-terminal helix forms a hydrogen bond with the main chain carbonyl oxygen of Ala104 of the neighboring subunit. Differences in this interaction may correlate with the different dissociation rates of inhibitors from the MTANs (Figure 3). Structural and mutagenesis studies will be needed to investigate these interactions.

The binding of most high-affinity inhibitors to MTANs displays favorable enthalpy and entropy, with two exceptions showing small entropic penalties. The related human MTA phosphorylase, *h*MTAP, is profoundly different and displays highly favorable entropy with a small penalty in enthalpy in its binding of transition state analogues.[9] The transition state analogues described here for MTANs are also transition state analogues for *h*MTAP; thus, the thermodynamic binding differences relate to

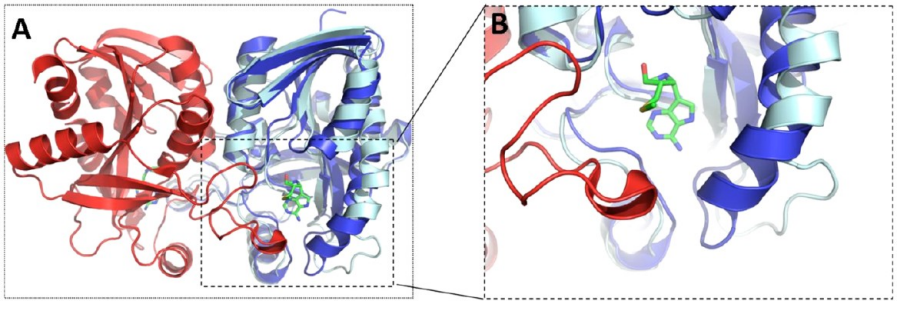

Figure 9. Crystal structure of *Ec*MTAN. (A) *Ec*MTAN dimer with MT-DADMe-ImmA bound in the active site shown as a red and blue ribbon (PDB entry 1Y6Q). The apo *Ec*MTAN monomer is shown as a cyan ribbon (PDB entry 1Z5P). (B) Close-up of the loop to helix conformational change that occurs in apo vs liganded *Ec*MTAN. The extended helix (blue) of monomer A moves toward the 3_{10} helix of monomer B when *Ec*MTAN is bound to MT-DADMe-ImmA.

dx.doi.org/10.1021/bi3009938 | *Biochemistry* 2012, 51, 7541−7550

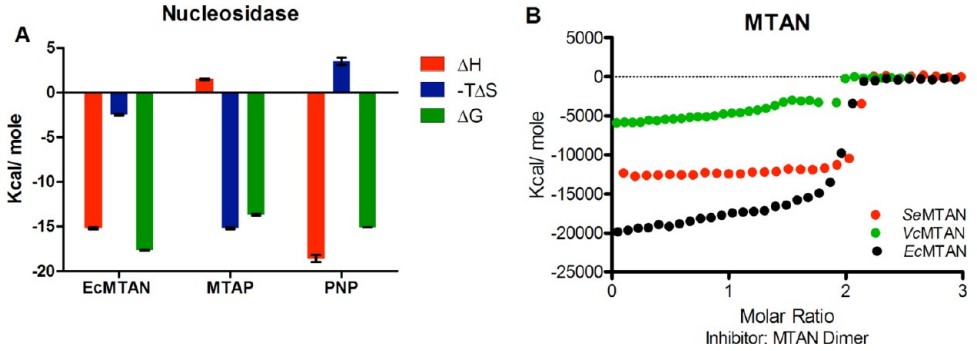

Figure 10. Thermodynamic profiles for binding of transition state analogues to *N*-ribosyltransferases (nucleosidases). (A) Comparison of the thermodynamic titration data for binding of MT-DADMe-ImmA to *Ec*MTAN and *h*MTAP or binding of DADMe-ImmH to *h*PNP. (B) Comparison of the experimental enthalpic contributions for binding of MT-DADMe-ImmA to the three MTANs.

protein architecture, not inhibitor structure. Despite the MTAP and MTAN enzymes sharing a common substrate (MTA) and similar transition states, binding the same transition state analogues follows distinct pathways along the energetic binding landscape. Human purine nucleoside phosphorylase (*h*PNP) is a structural homologue of *h*MTAP and also catalyzes phosphorolysis of a purine nucleoside N-ribosidic bond. *h*PNP binds to its transition state analogues with a highly favorable enthalpy and pays a penalty in entropy because of system organization (Figure 10).[10] The combined favorable enthalpy and entropy contributions to binding of the best transition state analogues to MTAN result in extremely tight binding with the best K_i* far surpassing that of either PNP or *h*MTAP.

CONCLUSIONS

The binding of transition state analogues to MTANs display tight binding constants as a result of combined favorable enthalpy and entropy components. The thermodynamic profile for binding transition state analogues to MTANs is distinct from those of *h*MTAP, which shares the substrate and a similar transition state. The thermodynamics also differ from those for binding of transition state analogues to *h*PNP, which also has a ribocation transition state. The thermodynamic contributions of transition state analogue binding to closely related MTANs from different bacterial species also differ, despite the similarity in structure and sequence identity. Although the catalytic sites are nearly identical, minute differences in the position or motion of first-sphere catalytic residues may partially account for the different thermodynamic signatures. Alternatively, distinct energetic contributions to transition state analogue binding could be indicative of enzyme-specific protein-wide dynamic contributions to system thermodynamics dominating local active site contributions. While dynamical effects are not directly observed in binding studies, something other than static structural elements is likely to contribute to the energetic differences reported here. In enzymes with 95% identical sequences yet producing distinct thermodynamic profiles, it is reasonable to propose differences in protein dynamics between free and bound states for the individual proteins to account for altered entropic contributions.

ASSOCIATED CONTENT

Supporting Information

Additional methods, synthesis of radiolabeled [^{14}C]MT-DADMe-ImmA, and sequence alignment of *Ec*MTAN (*Ec*), *Se*MTAN (*Se*), and *Vc*MTAN (*Vc*) generated using ClustalW2 (Figure S1). This material is available free of charge via the Internet at http://pubs.acs.org.

AUTHOR INFORMATION

Corresponding Author

*Telephone: (718) 430-2813. Fax: (718) 430-8565. E-mail: vern.schramm@einstein.yu.edu.

Notes

The authors declare no competing financial interest.

ABBREVIATIONS

MTA, 5′-methylthioadenosine; MTR, 5-methylthioribose; MTAN, MTA nucleosidase; MTAP, MTA phosphorylase; PNP, purine nucleoside phosphorylase; ImmA, Immucillin-A; DADMe, 4′-deaza-1′-aza-2′-deoxy-1′-(9-methylene); *Ec*MTAN, *E. coli* MTAN; *Vc*MTAN, *V. cholerae* MTAN; *Se*MTAN, *S. enterica* MTAN; PDB, Protein Data Bank.

REFERENCES

(1) Sperandio, V., Torres, A. G., Jarvis, B., Nataro, J. P., and Kaper, J. B. (2003) Bacteria-host communication: The language of hormones. *Proc. Natl. Acad. Sci. U.S.A. 100*, 8951−8956.

(2) Sperandio, V., Torres, A. G., Giron, J. A., and Kaper, J. B. (2001) Quorum Sensing Is a Global Regulatory Mechanism in Enterohemorrhagic *Escherichia coli* O157:H7. *J. Bacteriol. 183*, 5187−5197.

(3) Clarke, M. B. (2006) The QseC sensor kinase: A bacterial adrenergic receptor. *Proc. Natl. Acad. Sci. U.S.A. 103*, 10420−10425.

(4) Singh, V., Lee, J. E., Nunez, S., Howell, P. L., and Schramm, V. L. (2005) Transition state structure of 5′-methylthioadenosine/S-adenosylhomocysteine nucleosidase from *Escherichia coli* and its similarity to transition state analogues. *Biochemistry 44*, 11647−11659.

(5) Singh, V., Luo, M., Brown, R. L., Norris, G. E., and Schramm, V. L. (2007) Transition-state structure of *Neisseria meningitides* 5′-methylthioadenosine/S-adenosylhomocysteine nucleosidase. *J. Am. Chem. Soc. 129*, 13831−13833.

(6) Singh, V., and Schramm, V. L. (2007) Transition-state analysis of *S. pneumoniae* 5′-methylthioadenosine nucleosidase. *J. Am. Chem. Soc. 129*, 2783−2795.

(7) Gutierrez, J. A., Luo, M., Singh, V., Li, L., Brown, R. L., Norris, G. E., Evans, G. B., Furneaux, R. H., Tyler, P. C., Painter, G. F., Lenz, D. H., and Schramm, V. L. (2007) Picomolar Inhibitors as Transition-State Probes of 5′-Methylthioadenosine Nucleosidases. *ACS Chem. Biol. 2*, 725−734.

(8) Evans, G. B., Furneaux, R. H., Lenz, D. H., Painter, G. F., Schramm, V. L., Singh, V., and Tyler, P. C. (2005) Second Generation Transition State Analogue Inhibitors of Human 5′-Methylthioadenosine Phosphorylase. *J. Med. Chem. 48*, 4679−4689.

(9) Guan, R., Ho, M.-C., Brenowitz, M., Tyler, P. C., Evans, G. B., Almo, S. C., and Schramm, V. L. (2011) Entropy-Driven Binding of

Picomolar Transition State Analogue Inhibitors to Human 5′-Methylthioadenosine Phosphorylase. *Biochemistry 50*, 10408−10417.
(10) Edwards, A. A., Mason, J. M., Clinch, K., Tyler, P. C., Evans, G. B., and Schramm, V. L. (2009) Altered Enthalpy−Entropy Compensation in Picomolar Transition State Analogues of Human Purine Nucleoside Phosphorylase. *Biochemistry 48*, 5226−5238.
(11) Wolfenden, R. (1976) Transition State Analogue Inhibitors and Enzyme Catalysis. *Annu. Rev. Biophys. Bioeng. 5*, 271−306.
(12) Schramm, V. L. (1998) Enzymatic transition states and transition state analog design. *Annu. Rev. Biochem. 67*, 693−720.
(13) Evans, G. B., Furneaux, R. H., Schramm, V. L., Singh, V., and Tyler, P. C. (2004) Targeting the Polyamine Pathway with Transition-State Analogue Inhibitors of 5′-Methylthioadenosine Phosphorylase. *J. Med. Chem. 47*, 3275−3281.
(14) Wilkins, M. R., Gasteiger, E., Bairoch, A., Sanchez, J. C., Williams, K. L., Appel, R. D., and Hochstrasser, D. F. (1999) Protein identification and analysis tools in the ExPASy server. *Methods Mol. Biol. 112*, 531−552.
(15) Emsley, P., and Cowtan, K. (2004) Coot: Model-building tools for molecular graphics. *Acta Crystallogr. D60*, 2126−2132.
(16) Williams, D. H., Stephens, E., O'Brien, D. P., and Zhou, M. (2004) Understanding Noncovalent Interactions: Ligand Binding Energy and Catalytic Efficiency from Ligand-Induced Reductions in Motion within Receptors and Enzymes. *Angew. Chem., Int. Ed. 43*, 6596−6616.
(17) Gutierrez, J. A., Crowder, T., Rinaldo-Matthis, A., Ho, M. C., Almo, S. C., and Schramm, V. L. (2009) Transition state analogs of 5′-methylthioadenosine nucleosidase disrupt quorum sensing. *Nat. Chem. Biol. 5*, 251−257.
(18) Lee, J. E., Singh, V., Evans, G. B., Tyler, P. C., Furneaux, R. H., Cornell, K. A., Riscoe, M. K., Schramm, V. L., and Howell, P. L. (2005) Structural rationale for the affinity of pico- and femtomolar transition state analogues of *Escherichia coli* 5′-methylthioadenosine/S-adenosylhomocysteine nucleosidase. *J. Biol. Chem. 280*, 18274−18282.
(19) Copeland, R. A., Pompliano, D. L., and Meek, T. D. (2006) Drug-target residence time and its implications for lead optimization. *Nat. Rev. Drug Discovery 5*, 730−739.
(20) Garvey, E. P. (2010) Structural Mechanisms of Slow-Onset, Two-Step Enzyme Inhibition. *Curr. Chem. Biol. 4*, 64−73.
(21) Sullivan, S. M., and Holyoak, T. (2008) Enzymes with lid-gated active sites must operate by an induced fit mechanism instead of conformational selection. *Proc. Natl. Acad. Sci. U.S.A. 105*, 13829−13834.